Surfactant-Encapsulated Europium-Substituted Heteropolyoxotungstates: Structural Characterizations and Photophysical Properties

Weifeng Bu, Haolong Li, Wen Li, Lixin Wu,* Chunxi Zhai, and Yuqing Wu

Key Laboratory for Supramolecular Structure and Materials of Ministry of Education, Jilin University, Changchun 130012, People's Republic of China

Received: April 4, 2004; In Final Form: June 3, 2004

The surfactant-encapsulated europium-substituted heteropolyoxotungstates (Eu-POMs), $(DODA)_{10}H[Eu(H_2O)(PW_{11}O_{39})_2]\cdot 17H_2O$ (SEC-2, DODA: dimethyl dioctadecylammonium), $(DODA)_{12}H_3[Eu(BW_{11}O_{39})_2]\cdot 13H_2O$ (SEC-3), and $(DODA)_9[EuW_{10}O_{36}]\cdot 9H_2O$ (SEC-4), are structurally characterized in detail and their photophysical behavior is investigated. The DODA alkyl chains of SEC-2, SEC-3, and SEC-4 are well ordered. The solid-state SEC-2 and SEC-3 show two different lamellar structures with interlayer distances of 3.6 and 4.9 nm, respectively, but SEC-4 only offers a much shorter lamellar distance of 3.2 nm. In the case of short periodicities, it is considered that the alkyl chains are partially interdigitated, and the interdigitated length may reach 1.3 nm in SEC-2 and SEC-3. Of difference is that DODA alkyl chains are almost fully interdigitated in SEC-4. On the basis of a series of SECs with 15, 13, 11, and 9 negative charges, we suggest that the DODA molecule can occupy a minimum area of 0.57 ± 0.04 nm^2 on the surface of polyoxometalate. SEC-2, SEC-3, and SEC-4 exhibit the characteristic $^5D_0 \rightarrow {}^7F_j$ ($j = 0, 1, 2, 3, 4$) Eu^{3+} emission. The photophysical properties of Eu-POMs have been modified such as spectra, lifetimes, and intramolecular energy transfer from heteropolytungstate ligands to Eu^{3+} ion after encapsulating them with DODA. Therefore, the nanostructures of Eu-POMs can influence their photophysical behavior. X-ray photoelectron spectroscopy shows that the amphiphiles strongly impact the electronic properties of Eu-POMs, which rationally explains the various photophysical properties before and after the encapsulation with cationic surfactants. The controllable relationship between the nanostructures and the photophysical properties of Eu-POMs is significant for the future realization of POM-based functional devices.

Introduction

Supramolecular self-organization has provided an effective way to produce ordered functional materials with complex molecular structures.[1] In recent years, an important topic of functional material designs focuses on the incorporation of inorganic functional polyelectrolytes into the matrixes of amphiphiles based on electrostatic interactions. On the basis of ionic exchange, one-dimensional negatively charged conducting $[Mo_3Se_3^-]_\infty$ had been encapsulated by cationic surfactants, which form surfactant-induced mesoscopic assemblies.[2] Various anion surfactants can displace the counteranion of the one-dimensional mixed-valence complexes, forming lipid-packaged mixed-valence metal nanowires.[3−5] These organic/inorganic complexes could be dispersed or dissolved in organic media such as chloroform, dichloromethane, and benzene. In this system, incorporation of amphiphiles as the counteranion not only provides solubility to one-dimensional mixed-valence metal chains, but also remarkably impacts their electronic structures.[4] The materials produced from a series of double-tail ammoniums and inorganic crown $[Ni_3P_3S_{12}]^{3-}$ represent stable room-temperature liquid-crystalline materials. Interestingly, these complexes show a reversible solid−solid transition from discotic arrangements of clusters toward inorganic polymers (by heating) and back to the crown species (by solvent).[6] Polyoxometalates (POMs) are intriguing nanosized clusters due to their structural, chemical, and electronic versatility.[7,8] The cationic surfactants can replace the counterions of POMs, resulting in the surfactant-encapsulated clusters (SECs).[9−21] SECs possess a hydrophobic shell and an encapsulated hydrophilic POM core with a well-defined composition, and are soluble in nonpolar solvents such as chloroform, benzene, and toluene. Well-ordered thin films of SECs are readily prepared by LB technique and solvent-casting method. These above-mentioned systems have combined solid-state inorganic chemistry and surfactant chemistry, which can design organic/inorganic hybrid materials soluble in organic solvents. That is, the inorganic clusters are enwrapped with a water-insoluble shell composed of organic molecules so that the surfactant-encapsulated inorganic polyelectrolytes are soluble in organic media. These supramolecular assemblies can be processed into thin films by spin coating, simple casting, and LB techniques. Therefore, the present methodology is offering promising approaches toward new supramolecular soft materials containing inorganic functional units.

We have synthesized and characterized the surfactant-encapsulated europium-substituted heteropolyoxotungstate (Eu-POM), $(DODA)_{11}H_2[Eu(H_2O)_4(SiW_{11}O_{39})_2]$ (DODA: dimethyl dioctadecylammonium), SEC-1, which exhibits the characteristic $^5D_0 \rightarrow {}^7F_j$ ($j = 0, 1, 2, 3, 4$) Eu^{3+} emission.[15] The solution, solid state, solvent-casting films, and LB films of SEC-1 show different photophysical behaviors. Of significance is that the photophysical properties of SEC-1 in its thin films can be modified by careful changes of the lamellar distance in the different organized thin films, for example, LB and solvent-casting films. A model study has been presented for the

* To whom correspondence should be addressed. Fax: +86 431-5193421. E-mail: wulx@jlu.edu.cn.

10.1021/jp0485237 CCC: $27.50
Published on Web 07/29/2004

TABLE 1: The Assignments of Infrared Spectra of SEC-8, SEC-10, and SEC-11 in Their Solid State According to Ref 33

SEC-1[a]	SEC-2	SEC-3	SEC-4	assignments[b]
3469	3475	3470	3472	O−H antisym str
2956	2956	2956	2956	CH_3 antisym str
2919	2919	2919	2918	CH_2 antisym.str
2849	2849	2849	2850	CH_2 sym.str
1635	1630	1640	1635	O−H scissoring
1484	1484	1484	1484	CH_2N scissoring
1468	1468	1468	1468	CH_2 scissoring
1379	1380	1379	1380	CH_3 scissoring
998		994		W−O_d sym str
	1101			
	1052			
944	952	944	945	W−O_d antisym str
890	889	887	870	W−O_b−W antisym str
	826	833	842	W−O_c−W antisym str
816			815	W−O_c−W antisym str
772	784	780	780	W−O_c−W antisym str
721	726	720	722	CH_2 rocking

[a] Reference 15. [b] Antisym str = antisymmetrical stretching; sym str = symmetrical stretching.

TABLE 2: The Summary of the O → W LMCT Bands, Measured Intensity Ratios $I(^5D_0 \rightarrow {}^7F_2)/I(^5D_0 \rightarrow {}^7F_1)$, Luminescent Lifetimes, and Number of Coordinated Water Molecules for POM-1a, POM-2a, POM-3a, and POM-4a in Their Solid States at Room Temperature

solid state	LMCT band	$I(^5D_0 \rightarrow {}^7F_2)/I(^5D_0 \rightarrow {}^7F_1)$	lifetime (ms) from H_2O	lifetime (ms) from D_2O	q[a]
SEC-1	341	2.5	0.844, 0.194	2.85, 0.471	0.9, 5.0
POM-1	*b*	1.13	2.4	2.4	0
SEC-2	345	1.9	0.76	2.24, 0.241	0.9
POM-2	*b*	1.11	2.5		0
SEC-3	350	1.52	1.15	1.71, 0.485	0
POM-3	*b*	1.13	1.8		0
SEC-4	284	0.34	2.1	1.8	0
POM-4[c]	317	1.1	2.9	3.1	0

[a] q, number of coordinated water molecules. [b] Not detected, from refs 24 and 25. [c] From ref 27.

controllable relationship between the nanostructures and properties of functional POMs. Interestingly, the photophysical properties of SEC-1 such as excited, emissive spectra, lifetime, and energy transfer from the oxygen-to-tungsten charge transfer (O→W LMCT) state to Eu^{3+} ion are different from those of $K_{13}[Eu(SiW_{11}O_{39})_2]\cdot 20H_2O$ (POM-1, see Table 2). Similar differences were observed between $Na_9[EuW_{10}O_{36}]\cdot 32H_2O$ and $[C_{16}TA]_9[EuW_{10}O_{36}]$ ($C_{16}TA$: hexadecyltrimethylammonium).[20] LB films constructed from Langmuir monolayers adsorbing Eu-POMs in the aqueous subphase also show the distinct photophysical behaviors from those of the naked Eu-POMs.[22,23] The electronic properties of the encapsulated nanoclusters come from Eu-POMs. On the basis of these investigations, we therefore ask what is the precise mechanism concerning the changes of electronic configurations after encapsulating Eu-POMs.

Eu-POMs, $K_{11}[Eu(PW_{11}O_{39})_2]\cdot 13H_2O$ (POM-2), $K_{15}[Eu(BW_{11}O_{39})_2]\cdot 16H_2O$ (POM-3), and $Na_9[EuW_{10}O_{36}]\cdot 32H_2O$ (POM-4), show the characteristic $^5D_0 \rightarrow {}^7F_j$ ($j = 0, 1, 2, 3, 4$) transitions of Eu^{3+} emission.[24−27] And the O → W LMCT bands of POM-1, POM-2, and POM-3 illustrate a strong temperature dependence,[24,25] whereas POM-4 gives a small temperature dependence of quantum yield (with its high value) of the intramolecular energy transfer from $[W_5O_{18}]^{6-}$ ligands to Eu^{3+}.[26,27] This is associated with the competition between the thermal relaxation of the O → W LMCT states and the energy transfer to Eu^{3+}.[24,25] In $[Eu(PW_{11}O_{39})_2]^{11-}$ (POM-2a) and $[Eu(BW_{11}O_{39})_2]^{15-}$ (POM-3a), the Eu^{3+} ion is coordinated respectively by two lacunary

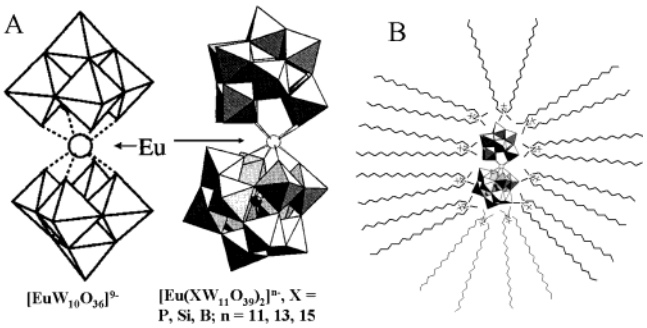

Figure 1. (A) Coordination polyhedral representations of POM-1, POM-2, POM-3, and POM-4 clusters encapsulated in this study; (B) the schematic drawing of the chemical structure of SEC-1 that shows a core−shell structure, from ref 15.

Keggin-type $[PW_{11}O_{39}]^{7-}$ and $[BW_{11}O_{39}]^{9-}$ groups through eight oxygen atoms and forms an Archimededian antiprism.[28] The polytungstate groups consisting of distorted tungstate octahedra have approximate C_{4v} (actual C_s) symmetry. $[EuW_{10}O_{36}]^{9-}$ (POM-4a) consists of two lacunary Lindqvist-type $[W_5O_{18}]^{6-}$ linked by Eu^{3+}, and shows C_{4v} symmetry.[26] In this article, we synthesized three surfactant-encapsulated Eu-POMs, $(DODA)_{10}H[Eu(H_2O)(PW_{11}O_{39})_2]\cdot 17H_2O$ (SEC-2), $(DODA)_{12}H_3[Eu(BW_{11}O_{39})_2]\cdot 13H_2O$ (SEC-3), and $(DODA)_9[EuW_{10}O_{36}]\cdot 9H_2O$ (SEC-4),[17] bearing a core−shell ellipsoid as schematically drawn in Figure 1, and carried on a comprehensive investigation of SEC-2, SEC-3, and SEC-4 in both their structures and photophysical behavior. The photophysical properties of Eu-POMs can be easily modified by improvement of their surface chemical properties. That is to say, the different nanostructures, i.e., the encapsulated and naked Eu-POMs, show the different photophysical properties. We try to clarify why the photophysical properties of Eu-POMs are different after changing their nanostructures by the encapsulation.

Experimental Section

Preparation. POM-2 and POM-3 were freshly prepared according to literature procedures.[29] Dimethyl dioctadecylammonium bromide (DODA·Br, 99%) was purchased from Acros Organics and used as received. SEC-2 and SEC-3 were synthesized by the previously reported procedures.[15] SEC-1 and SEC-4 have been synthesized and characterized in our previous work, refs 15 and 17, respectively. Eu-POMs were dissolved in aqueous solution (pH 6), and then a chloroform solution of DODA·Br was added with stirring. The initial molar ratios of DODA·Br to POM-2 and POM-3 were controlled at 10:1 and 11:1, respectively. The organic phases were separated, and both SEC-2 and SEC-3 were obtained by evaporating the chloroform to dryness. Then the samples were further dried in a vacuum until the weight remained constant. For SEC-2: ^1H NMR ($CDCl_3$, 500 MHz) δ 0.88 (t, $J = 7.5$ Hz, 6H, CH_3), 1.25 (m, 60H, CH_2), 1.60 (br, 4H, CH_2), 3.25 (br, 10H, NCH_3 and NCH_2); Fourier transformation infrared spectroscopy (FTIR) (KBr, cm^{-1}) ν 3475, 2956, 2919, 2849, 1630, 1484, 1468, 1380, 1101, 1052, 952, 889, 826, 784, 726, 517. Anal. Calcd for SEC-2 ($C_{380}H_{837}N_{10}O_{96}W_{22}P_2Eu$, 11342.38): C 40.24, H 7.44, N 1.23. Found: C 39.99, H 7.14, N 1.29. The first thermogravimetric analysis (TGA) stage of SEC-2 (temperature range: 20 to 200 °C) corresponds to the loss of the crystalline water (2.8%), and the calculated number of crystalline water is about 17. Combining the TGA and elemental analysis, SEC-2 should correspond to the formula $(DODA)_{10}H[Eu(H_2O)(PW_{11}O_{39})_2]\cdot 17H_2O$. For SEC-3: ^1H NMR ($CDCl_3$, 500 MHz) δ 0.88 (t, J

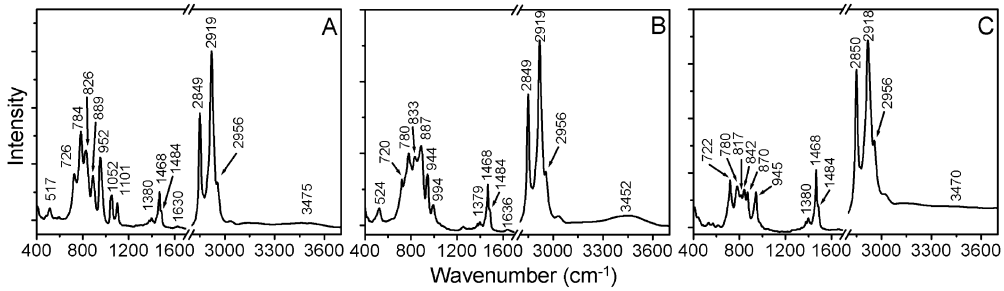

Figure 2. FT-IR absorption spectra of SEC-2 (A), SEC-3 (B), and SEC-4 (C) at the solid state in KBr pellets.

= 7.5 Hz, 6H, CH_3), 1.26 (m, 60H, CH_2), 1.72 (br, 4H, CH_2), 3.41 (br, 6H, NCH_3), 3.51 (br, 4H, NCH_2); FTIR (KBr, cm^{-1}) ν 3452, 2956, 2919, 2849, 1636, 1484, 1468, 1379, 994, 944, 887, 833, 780, 720, 524. Anal. Calcd for SEC-3 ($C_{456}H_{989}N_{12}O_{91}W_{22}B_2Eu$, 12316.15): C 44.47, H 8.09, N 1.37. Found: C 44.49, H 8.05, N 1.28. The first TGA stage of SEC-3 (temperature range: 20 to 180 °C) corresponds to the loss of the crystalline water (1.8%), and the calculated number of crystalline water is about 13. Combining the TGA and elemental analysis, SEC-3 should correspond to the formula $(DODA)_{12}H_3[Eu(BW_{11}O_{39})_2]\cdot 13H_2O$.

Measurements. FT-IR spectra were performed on a Bruker IFS66V FT-IR spectrometer equipped with a DGTS detector for the solid-state SECs (32 scans). The spectra were recorded with a resolution of 4 cm^{-1}. ^1H NMR spectra (TMS) were recorded on a Bruker UltraShield 500 MHz spectrometer. Luminescent measurements were performed on a Spex FL=2T2 spectrophotometer, using a xenon lamp as the excitation source. The luminescent lifetimes were recorded on a Spex 1934D-phosphorescence spectrophotometer. The solid-state SECs were characterized by wide-angle X-ray diffraction, which was carried out on a Rigaku X-ray diffractometer (*D*/max rA, using Cu Kα radiation of a wavelength of 1.542 Å). The element analysis was measured on a Flash EA1112 from ThermoQuest Italia S.P.A. X-ray photoelectron spectroscopy (XPS) was performed on a VG ESCALAB MK-III spectrometer at a pressure of 10^{-7} Pa. The Al Kα (1486.5 eV) was used as the excitation source, and the resolution of scans is 0.05 eV. The binding energy of the sample was corrected on the basis of the adventitious carbon (C1s) to 284.6 eV. The TGA was measured on a Perkin-Elmer 7 series thermal analysis system. All spectroscopic measurements were carried out at room temperature.

Results and Discussion

Characterization. Similar to SEC-1, SEC-2, SEC-3, and SEC-4 are immiscible in water, but readily dissolve in organic media such as benzene, toluene, or chloroform. In contrast, POM-2, POM-3, and POM-4 are only soluble in water. This indicates that POM-2a, POM-3a, and POM-4a have been successfully encapsulated with DODA. These organic/inorganic hybrids are characterized by elemental analysis, FTIR, ^1H NMR, and TGA (see the Experimental Section). TGA shows that there is some crystal water in SEC-2, SEC-3, and SEC-4. Combining the element and thermogravimetric analyses, we offer the chemical formulas of SEC-2 and SEC-3. These complexes are stable in air, but may lose some or all of their crystal water upon storage in air.

^1H NMR spectra of SEC-2, SEC-3, and SEC-4 confirm the presence of surfactants in the encapsulated clusters. In contrast to the resonance signals of DODA·Br alone, those of DODA in SEC-2 are changed as follows. (1) The signal of the *N*-methyl proton is significantly broadened and shifted to high field by δ 0.19. (2) The proton signal of *N*-methylene, which should be split into a triplet, shows up as a considerably broadened singlet and shifts toward high field by δ 0.3. We observe the similar broadening of the DODA resonance signals in SEC-3, but their chemical shifts are hardly changed. The proton resonance signals of DODA in SEC-4 shift toward high field more significantly than in other SECs, for example, N-CH_2 0.73 ppm, N-CH_3 0.29 ppm, and β-CH_2 0.12 ppm. The peak broadening and shift should result from the strong electrostatic interaction between surfactants and POMs. That is, the surfactants are immobilized on the surface of POMs in the organic phase, and to some extent, their mobility is confined, especially for their head parts. The shift and broadening of the resonance signals of SEC-2, SEC-3, and SEC-4 are different from one another, also those in the literatures,[9,11,14−16] indicating the different mobility of DODAs in the different SECs. Remarkable shifts of the proton resonance signals in SEC-4 may be attributed to a rather sparsely occupied area of DODA on the surface of POM-4a (0.53 nm^2). ^{183}W NMR measurements for SECs in $CDCl_3$ failed.[15] Similar results are also observed by Pope et al., which were thought to be due to the solution's high viscosity and consequently the lower mobility of POMs.[30]

In the IR spectra of the solid-state SEC-2 and SEC-3 (Figure 2A,B), bands at 2919 and 2849 cm^{-1} are assigned to CH_2 antisymmetric and symmetric stretching modes of DODA alkyl chains, respectively. And the CH_2 antisymmetric and symmetric stretching bands of DODA in SEC-4 appear at 2918 and 2850 cm^{-1}, respectively (Figure 2C). These bands are consistent with those of crystalline DODA·Br (2918 and 2850 cm^{-1}). The frequencies of the CH_2 stretching bands are sensitive to the conformation of a hydrocarbon chain: low frequencies (2918 and 2848 cm^{-1}) of the bands are characteristic of a highly ordered alkyl chain, while their upward shifts (2927 and 2856 cm^{-1}) are indicative of the increase in conformational disorder, i.e., gauche conformers, in the hydrocarbon chain.[31,32] The fact that the CH_2 stretching bands appear at 2919 and 2949 cm^{-1} in the infrared spectra suggests the DODA alkyl chains are well-ordered in the solid-state SEC-2, SEC-3, and SEC-4. However, this does not mean the alkyl chains are of a fully extended conformation. POM-1a, POM-2a, and POM-3a consist of two lacunary Keggin structures of $[XW_{11}O_{39}]^{n-}$ (X = P, Si, and B; n = 7, 8, and 9) linked by a europium ion.[28] By considering the radius (0.52 nm)[33] of Keggin-type POMs, the surface area of POM-2a and POM-3a should be around 6.8 nm^2. Thus every DODA in both SEC-2 and SEC-3 will occupy an area of 0.68 and 0.57 nm^2, respectively. The latter is consistent with the lateral area (0.567 nm^2) in the crystal structure of DODA·Br,[34] while the former is slightly larger than its lateral area. Since POM-4a consists of two lacunary Lindqvist-type $[W_5O_{18}]^{6-}$ linked by Eu^{3+},[26] its surface area should be around 4.8 nm^2 based on the diameter (0.87 nm) of Lindqvist-type POMs.[26] Therefore, every DODA in SEC-4 will occupy an area of 0.53

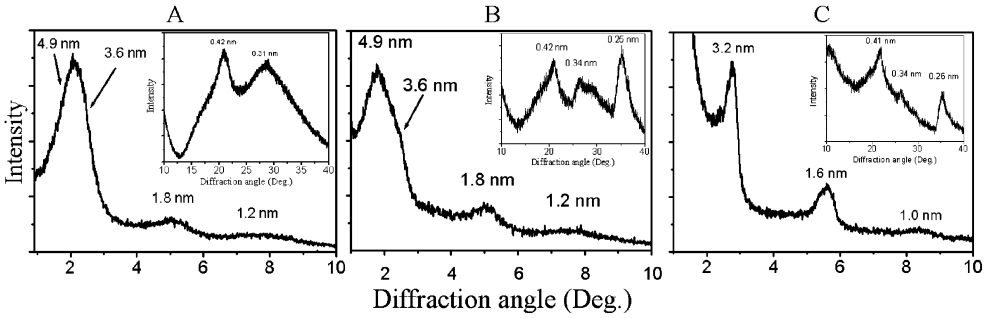

Figure 3. X-ray diffraction patterns of SEC-2 (A), SEC-3 (B), and SEC-4 (C).

nm^2, which is similar to the lateral area of DODA·Br. This result shows that DODA alkyl chains pack more closely on the surface of POM-4a, rationally explaining those remarkable shifts of the proton resonance signals in SEC-4. X-ray analysis of crystalline DODA·Br indicates that one of its two hydrocarbon chains is bent at an almost right angle in the third carbon atom, while after that carbon, both chains have a trans-zigzag conformation with their molecular planes parallel to each other.[34] On the basis of their similar lateral areas and IR frequencies, the conformations of DODA in SEC-2, SEC-3, and SEC-4 are similar to that of crystalline DODA·Br. The peaks at 2956 and 1379 cm^{-1} should be attributed to CH_3 antisymmetric stretching and deformation modes, respectively. The band at 1468 cm^{-1} is assigned to a CH_2 scissoring mode. The shoulder peaks at 1484 cm^{-1} may result from the interaction of the CH_2 groups with N^+, which leads to a change of charge distribution of the α-carbon atom of SEC-2, SEC-3, and SEC-4.[35,36] Strong bands are observed below 1000 cm^{-1} for POM-2a, POM-3a, and POM-4a vibrations.[33] The detailed assignments are summarized in Table 1.

Further evidence for the conformational order of DODAs comes from X-ray diffraction of the solid-state SEC-2, SEC-3, and SEC-4. Figure 3A (inset) represents Bragg peaks at 21° and 28.7°, corresponding to a spacing of 0.42 and 0.31 nm, respectively. The former means that DODA alkyl chains pack closely. Both Figure 3B (inset) and Figure 3C (inset) show three spacings of 0.42, 0.34, and 0.26 nm, which agrees well with the lateral packing of DODA·Br in its crystal structure.[34] The X-ray diffraction pattern of SEC-3 (Figure 3B) shows four Bragg diffraction peaks at 1.8°, 2.45°, 4.96°, and 7.48°, corresponding to the spacings of 4.9, 3.6, 1.8, and 1.2 nm, respectively. The ratio of the latter three spacings suggests that the signals arise from a lamellar structure with a layer distance of 3.6 nm. Of note is that POM-3a is a peanut-shaped POM with a long-to-short axis ratio of 2:1; thus most of the DODAs are proposed to align along its long axis as shown in Figure 1B.[12,13,15] Crystalline DODA·Br possesses a lamellar structure with an interlayer distance of 3.811 nm.[34] Taking the short-axis diameter of POM-3a and the length of DODA into account, the total thickness of a single SEC-3 should be around 4.8 nm, which is consistent with the first spacing in the X-ray diffraction of SEC-3. The short layer distance should be attributed to the partially interdigitated DODA alkyl chains in SEC-3, and the interdigitated depth is estimated to be about 1.3 nm. Similar Bragg peaks are also present in SEC-1 and SEC-2. But the relative intensities of peaks at 4.9 nm are different and increase in the order as follows: SEC-2 < SEC-1 < SEC-3, corresponding to the order of the occupied areas of DODA on the surfaces of POM-2, POM-1, and POM-3 (0.68, 0.62, and 0.57 nm^2). Of difference is that SEC-4 possesses a lamellar structure with a spacing of 3.2 nm (Figure 3C). On the basis of the short-axis diameter of POM-4a and the length of DODA, the total thickness of a single

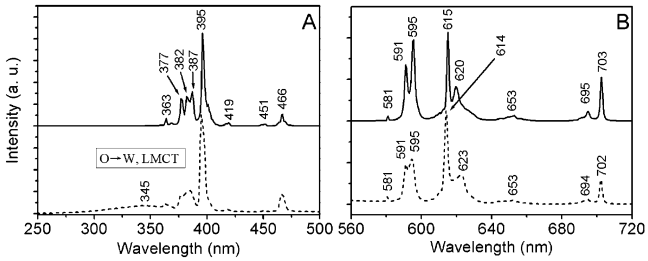

Figure 4. The excitation spectra (A) and the emission spectra (B) of POM-2 (full line) and SEC-2 (dashed line) at room temperature, respectively.

SEC-4 is estimated to be 4.7 nm, consistent with the spacing of its LB film (4.9 nm). The short layer distance may be attributed to the interdigitation of DODA alkyl chains, and the interdigitated depth is estimated to be 1.6 nm. By considering an interlayer distance of 3.811 nm in crystalline DODA·Br,[34] DODA alkyl chains are almost fully interdigitated in SEC-4.

This study and our previous result[15] raise an interesting question concerning how many DODA molecules can be electrostatically adsorbed on naked POMs. We have investigated four surfactant-encapsulated Eu-POMs so far with 15, 13, 11, and 9 negative charges. The cationic surfactant cannot replace all of the countercation in the SEC-1, SEC-2, and SEC-3, but can in the case of SEC-4, which is directly related to the number of charges of Eu-POMs. Therefore, we suggest that the DODA molecule can occupy a minimum area of 0.57 ± 0.04 nm^2 on the surface of POMs, which is consistent with the lateral area in the crystal structure of DODA·Br.[34] In the cases of high surface charge densities of POMs, for example, SEC-1, SEC-2, SEC-3, and SEC-4, DODA alkyl chains show well-ordered conformation and pack closely. However, in the case of a low surface charge density, for example, $(DODA)_{15}[H_3Mo_{57}V_6(NO)_6O_{189}(H_2O)_{12}(VO)_6]\cdot 13H_2O$, the surfactant is in the liquid expanded state and indicative of the disordered alkyl chains.[16] The packing structures of SECs are directly related to the surface charge density of POMs.[16] After describing the preparation and nanostructured characterization of SEC-2, SEC-3, and SEC-4, we will discuss the different photophysical properties between SECs and Eu-POMs and try to highlight the mechanism concerning the changes of electronic configurations after encapsulating Eu-POMs.

Photophysical Properties. Our previous work shows a sharp contrast of the photophysical properties between SEC-1 and POM-1. The excitation spectra of POM-2 and SEC-2 at room temperature exhibit sharp lines, corresponding to the characteristic transitions with the $4f^6$ shell of Eu^{3+}, as shown in Figure 4A. The detailed assignments are as follows: 363 ($^7F_0 \rightarrow {}^5D_4$), 376 ($^7F_0 \rightarrow {}^5G_4$), 381 ($^7F_0 \rightarrow {}^5G_3$), 385 ($^7F_0 \rightarrow {}^5G_2$), 395 ($^7F_0 \rightarrow {}^5L_6$), 416 ($^7F_0 \rightarrow {}^5D_3$), and 466 nm ($^7F_0 \rightarrow {}^5D_2$).[22,37] The relative intensity of the $^7F_0 \rightarrow {}^5L_6$ peak of SEC-2 is stronger

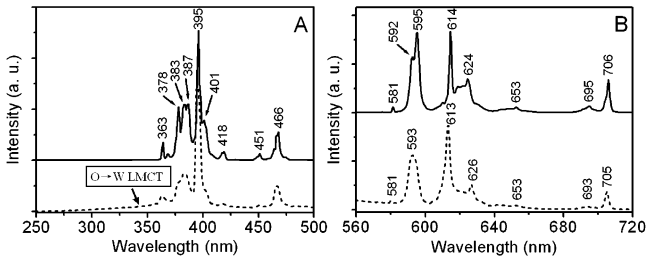

Figure 5. The excitation spectra (A) and the emission spectra (B) of POM-3 (full line) and SEC-3 (dashed line) at room temperature, respectively.

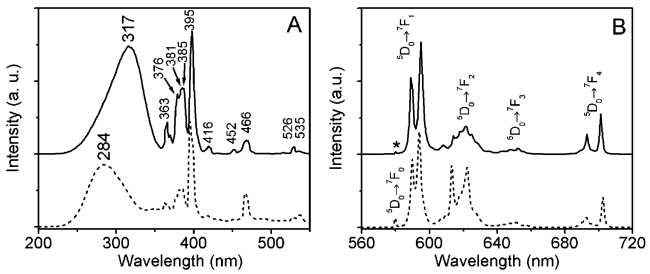

Figure 6. The excitation spectra (A) and the emission spectra (B) of POM-4 (full line) and SEC-4 (dashed line) at room temperature, respectively.

than that of POM-2. In contrast, the peaks due to $^7F_0 \rightarrow {}^5G_4$, $^7F_0 \rightarrow {}^5G_3$, and $^7F_0 \rightarrow {}^5G_2$ are weakened significantly in SEC-2. This should be ascribed to the different microenvironments of POM-2a. A broad band at 345 nm is clearly attributed to the O $\rightarrow$ W LMCT transition of SEC-2. Of difference is that the LMCT band for POM-2 cannot be observed at room temperature (Figure 4A).[24,25] Therefore, it can be inferred that the energy transfer from the O $\rightarrow$ W LMCT states to Eu^{3+} ions is more efficient and the communication between the O $\rightarrow$ W LMCT and excited Eu^{3+} levels is drastically increased in SEC-2. The excitation spectrum of the solid-state SEC-3 and SEC-4 also shows the characteristic transitions with the $4f^6$ shell of Eu^{3+}. Similar to POM-2, we cannot observe the O $\rightarrow$ W LMCT transition of POM-3 at room temperature.[24,25] The relative intensity of the O $\rightarrow$ W LMCT band (300−350 nm) of SEC-3 compared with its $^7F_0 \rightarrow {}^5L_6$ peaks becomes pretty low (Figure 5A). The excitation spectrum of POM-4 offers a strong O $\rightarrow$ W LMCT band at 317 nm, while the strong O $\rightarrow$ W LMCT band of SEC-4 appears at 284 nm (Figure 6A). Compared to POM-4, the O $\rightarrow$ W LMCT band of SEC-4 shows a blue shift of 33 nm.

The emission spectra of POM-2 and SEC-2 show the characteristic Eu^{3+} emission when excited at 395 nm (Figure 4B). The peaks are assigned to the $^5D_0 \rightarrow {}^7F_j$ ($j = 0, 1, 2, 3, 4$) transitions,[24,25] for instance, $^5D_0 \rightarrow {}^7F_0$, 581 nm; $^5D_0 \rightarrow {}^7F_1$, 591 and 594 nm; $^5D_0 \rightarrow {}^7F_2$, 614, 615, 620, and 623 nm; $^5D_0 \rightarrow {}^7F_3$, 653 nm; and $^5D_0 \rightarrow {}^7F_4$, 694, 695, 702, and 703 nm (Figure 4B). Similar $^5D_0 \rightarrow {}^7F_j$ ($j = 0, 1, 2, 3, 4$) transitions are also present in POM-3, SEC-3, POM-4, and SEC-4 (Figure 5B and Figure 6B). The strictly symmetrical forbidden emission, $^5D_0 \rightarrow {}^7F_0$, is not detected in the solid-state POM-4, but in the solid-state SEC-4 (Figure 6B). This result demonstrates that the microenvironment of the Eu^{3+} ion in POM-4 is changed from C_{4v} to C_s symmetry after the encapsulation. The photoexcitations at the O $\rightarrow$ W LMCT bands of SEC-2, POM-4, and SEC-4 result in an efficient intramolecular energy transfer from the heteropolyoxotungstates to Eu^{3+}, and their emission spectra show the characteristic $^5D_0 \rightarrow {}^7F_j$ ($j = 0, 1, 2, 3, 4$) transitions of Eu^{3+}. The $^5D_0 \rightarrow {}^7F_2$ transition is attributed to an electric dipole transition and is extremely sensitive to the chemical surroundings in the vicinity of Eu^{3+} ions. The intensity increases as the Eu−O covalency increases and environments become more asymmetrical. On the other hand, the $^5D_0 \rightarrow {}^7F_1$ transition is a magnetic dipole transition, and its intensity is almost independent of the changes of Eu^{3+} ion's chemical microenvironments. Therefore, the intensity ratio of the $^5D_0 \rightarrow {}^7F_2$ transition to the $^5D_0 \rightarrow {}^7F_1$ transition, referred to as $I(^5D_0\rightarrow{}^7F_2)/I(^5D_0\rightarrow{}^7F_1)$, is widely used to study the chemical microenvironments of Eu^{3+} ions.[38,39] The related data are summarized in Table 2. The intensity ratios of SEC-2, SEC-3, and SEC-4 are larger than those of their corresponding naked Eu-POM**s**, indicating that the encapsulation for Eu-POMs strongly affects the local environments of Eu^{3+} ions. Different intensity ratios, $I(^5D_0\rightarrow{}^7F_2)/I(^5D_0\rightarrow{}^7F_1)$, between SECs and Eu-POMs should be ascribed to different chemical environments.

The fluorescent lifetimes for Eu-POMs and SECsare summarized in Table 2. The fluorescent lifetime of POM-2 is 2.5 ms, while SEC-2 offers a much shorter lifetime of 0.76 ms. Replacement of OH oscillators by OD makes the vibronic deexcitation pathway exceedingly inefficient.[40] SEC-2a, prepared according to the procedures described in the Experimental Section except that POM-2 is dissolved in D_2O, gives a double-exponential decay (2.24 and 0.24 ms). Therefore, the shortened lifetime of SEC-2 should be due to the coordinated water to Eu^{3+}, and the number of water molecules coordinated to Eu^{3+} (q) can be calculated with an estimated uncertainty of 0.5, according to the following equation: $q = 1.05(1/\tau H_2O - 1/\tau D_2O)$ (1), where τH_2O and τD_2O are the experimental excited-state lifetimes in H_2O and D_2O environments, respectively.[40] The number of coordinated water molecules in SEC-2 is estimated to be about 1. POM-3 and SEC-3 have a fluorescent lifetime of 1.8[25] and 1.15 ms, respectively. POM-4 shows a single-exponential decay of the $^5D_0$ emission (2.9 ms),[27] while the fluorescent lifetime of SEC-4 is 2.1 ms. Similarly to SEC-2a, we also synthesized SEC-3a and SEC-4a. The former shows a double exponential decay of 1.71 and 0.485 ms, and the latter offers a lifetime of 1.8 ms. According to the equation, there is no coordinated water molecule in SEC-3 and SEC-4.

The O $\rightarrow$ W LMCT bands of POM-1, POM-2, and POM-3 cannot be detected at room temperature, but at low temperatures such as liquid nitrogen and liquid helium temperatures[24,25] because of the strong delocalization of the d^1 electron over $[XW_{11}O_{39}]^{n-}$ (X = P, Si, B; $n = 7, 8, 9$; corner-sharing WO_6 octahedra) via a thermal hopping mechanism, for example, rates of intramolecular electron transfer in $[PW_{12}O_{40}]^{4-}$ are $\sim 10^{11}$ to 10^{12} s^{-1} at room temperature.[41,42] However, the strong O $\rightarrow$ W LMCT transition can be found in the excited spectrum of POM-4 even at room temperature, which corresponds to its high quantum yield of the intramolecular energy transfer from the O $\rightarrow$ W LMCT excited state to Eu^{3+}.[27] This is due to the localization of the d^1 electron at the edge-sharing WO_6 octahedra in POM-4.[37] After encapsulating these Eu-POMs with DODA, we find that the photophysical properties of the europium-substituted heteropolyanion have been modified such as spectra, lifetimes, and intramolecular energy transfer from heteropolytungstate ligands to the Eu^{3+} ion (Table 2). These changes demonstrate that the d^1 electrons of SEC-1, SEC-2, SEC-3, and SEC-4 show more difficult delocalization than those of their corresponding Eu-POMs. Table 2 shows the changed degrees of their photophysical properties in the order of POM-3 < POM-4 $\approx$ POM-2 < POM-1. The electronic properties of SECs come from POMs. However, the photophysical properties can be easily changed by modifying the surface chemical properties

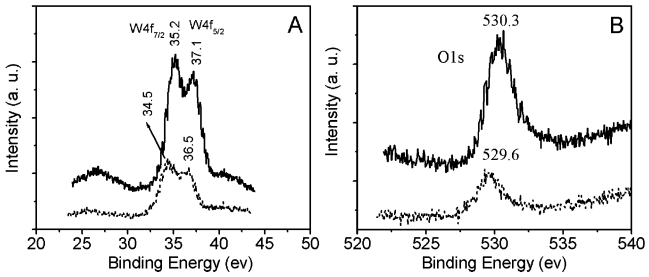

Figure 7. (A) W 4f and (B) O1s XP spectra of POM-1 (full line) and SEC-1 (dashed line) at room temperature, respectively.

of Eu-POMs with positive charged surfactants. Therefore, the organic amphiphilic cation not only plays a nanostructural role, but also has a strong effect on their photophysical behaviors. On the basis of the above analysis, it is important to study more systematically how the photophysical properties would depend on the nanostructures of Eu-POMs.

In fact, metal cations such as Rb^+, Cs^+, K^+, and Na^+ can coordinate on to POMs except for tetraalkylammoniums (R_4N^+) and Li^+ because of the larger hydrated radii of Li^+ and larger volumes of R_4N^+.[43] In the crystal structure of POM-4, the counterion, Na^+, is coordinated to the POM-4a polyoxoanion with a Na−O bond distance from 2.3 to 3.2 Å.[26] Up to now, there have been no single-crystal structures of POM-1, POM-2, and POM-3. In their similar single-crystal POM, $Cs_{12}[U(GeW_{11}O_{39})_2]\cdot 13-14H_2O$,[28] Cs^+ is coordinated onto $[U(GeW_{11}O_{39})_2]^{12-}$ with a Cs−O bond distance from 2.7 to 4.1 Å. $K-O_{ed}$, $K-O_{term}$, and $K-O_{cor}$ bond distances in Keggin-type single-crystal $K_6[CoW_{12}O_{40}]\cdot 11H_2O$ are 2.73, 2.74, and 3.93 Å, respectively.[44] Therefore, we believe that the K^+ ion can be coordinated onto the edge-sharing O, terminated O, and corner-sharing O atoms in the solid-state POM-1, POM-2, and POM-3. However, DODA cannot coordinate onto POMs in SEC-1, SEC-2, SEC-3, and SEC-4. Recent works concerning ion paring between cations and POM anions demonstrate that cations such as Cs^+, Rb^+, K^+, and Na^+ present within POMs act as an electronically more favorable pathway for electron transfer in POMs.[45−47] However, Li^+ and tetraalkylammonium cannot serve as conducting bridges between POMs.[43] On the basis of the above-mentioned analysis, the displacements of K^+ and Na^+ with DODA in POM-1, POM-2, POM-3, and POM-4 result in the weaker electron delocalization in SEC-1, SEC-2, SEC-3, and SEC-4. The direct evidence come from their XPS investigations.

XPS Investigations. X-ray photoelectron spectra have been measured for POM-1, SEC-1, POM-2, SEC-2, POM-3, SEC-3, POM-4, and SEC-4 in order to understand their unusual electronic properties and the differences of photophysical behavior after the encapsulation for Eu-POMs. The XP spectra of SEC-1 and POM-1 for W 4f core level signals are shown Figure 7A, which are composed of the $W4f_{7/2}$ spin−orbit components at lower and the $W4f_{5/2}$ ones at higher binding energies. The $W4f_{7/2}$ signals of SEC-1 and POM-1 appear at 34.5 and 35.2 eV, respectively. The binding energies are typical for tungsten(VI) centers,[48,49] which indeed is the highest oxidation state of the tungsten atoms in POM-1a. After the encapsulation for POM-1, the $W4f_{7/2}$ signal shifts toward lower binding energy by 0.7 eV. The O1s signals of SEC-1 and POM-1 reveal broad and complicated peaks at 529.6 and 530.3 eV, respectively. The shape of the peaks suggests that it is composed of more than one peak arising from the overlapping contribution of O_a, O_d, O_b, and O_c in POM-1a.[50] Similar to $W4f_{7/2}$ signals, the O1s signal also shifts toward lower binding energy by 0.7 eV. These low-energy shifts for $W4f_{7/2}$ and O1s signals strongly suggest that the d^1 electron in POM-1a becomes more difficult to delocalize after the encapsulation, which rationally explains the difference of the photophysical properties between POM-1 and SEC-1. Similar differences of XP spectra also can be observed between POM-2 and SEC-2, POM-3, and SEC-3, as well as POM-4 and SEC-4 (Table 3). But the changed degrees of their XP spectra are in the order of POM-3 < POM-4 ≈ POM-2 < POM-1, which corresponds to the changed degrees of their photophysical properties. Therefore, the photophysical and electronic properties of the different Eu-POMs, for example, POM-1a, POM-2a, POM-3a, and POM-4a, show the different dependences on their nanostructures.

TABLE 3: XPS Data for POM-1a, POM-2a, POM-3a, and POM-4a in Their Solid States at Room Temperature

	binding energy [eV]			
solid state	$W4f_{7/2}$	O1s	Δ $W4f_{7/2}$	Δ O1s
SEC-1	34.5	529.6	0.7	0.7
POM-1	35.2	530.3		
SEC-2	34.7	530.4	0.4	0.4
POM-2	35.1	530.8		
SEC-3	34.6	529.9	0.2	0.3
POM-3	34.8	530.2		
SEC-4	34.4	529.8	0.4	0.3
POM-4	34.8	530.1		

Conclusion

In this article we successively synthesized and characterized the surfactant-encapsulated europium-substituted heteropolyoxotungstates, $(DODA)_{10}H[Eu(H_2O)(PW_{11}O_{39})_2]\cdot 17H_2O$ (SEC-2), $(DODA)_{12}H_3[Eu(BW_{11}O_{39})_2]\cdot 13H_2O$ (SEC-3), and $(DODA)_9[EuW_{10}O_{36}]\cdot 9H_2O$ (SEC-4). The surface chemical properties of POMs become hydrophobic by the displacement of their countercations such as NH_4^+, K^+, and Na^+ with the cationic surfactants. The formed surfactant-encapsulated POM clusters (SECs) were believed to maintain the molecular entity of POMs in organic solvent. We have encapsulated a series of POMs with 16, 15, 13, 12, 11, and 9 negative charges,[12−17] and the surface areas of DODA are directly related to the surface charge density of POMs.[16] However, DODA molecules cannot always replace all countercations in Eu-POMs, for example, in SEC-1, SEC-2, and SEC-3. We, therefore, suggest that the minimum area of DODA absorbed on the POM surface is 0.57 ± 0.04 nm^2, consistent with the lateral area in the crystal structure of DODA·Br.[34] In a series of $[Eu(XW_{11}O_{39})_2]^{n-}$ (X = B, Si, and P; n = 15, 13, 11, respectively), the mesoscopic superstructures of SECs are directly related to the surface areas of DODA (Figure 3).

These materials exhibit the characteristic $^5D_0 \rightarrow {}^7F_j$ (j = 0, 1, 2, 3, 4) Eu^{3+} emission, and their photophysical properties such as excited, emissive spectra, lifetime, and energy transfer from the O → W LMCT state to Eu^{3+} ion are significantly different from those of their corresponding Eu-POMs (see Table 2). Although the electronic properties of SECs originate from Eu-POMs, the cationic surfactant plays a key role in modifying their photophysical behavior. K^+, Na^+, Rb^+, and Cs^+ can coordinate onto POMs and may act as a catalyst for electron transfer.[43,45,47] However, the cationic surfactants cannot, which makes Eu-POMs more difficult to delocalize in the amphiphilic matrixes. Herein, the cationic surfactant as countercations not only provides the solubility and nanosized supramolecular assemblies for POMs, but also exerts a significant influence on their electronic structures. Our work rationally explains the variety of photophysical properties between POMs/surfactant nanosturctured hybrids and the naked Eu-POMs described in

the literatures.[15,20,22,23] Similar relationships between the nanostructures and functional properties of POMs have also been observed in other systems. The ionic complexes between dendritic polyammonium and $[PO_4(WO(O_2)_2)_4]^{3-}$ are nanosized oxidation catalysts, and their catalytic properties depend on their nanostructures.[51] $[(Fe^{III}(H_2O)_2)_3(A\text{-}\alpha\text{-}PW_9O_{34})_2]^{9-}$ can be electrostatically bound on the cationic silica nanoparticles, forming POM-coated silica nanoparticle materials. This nanostructured hybrid as an active heterogeneous catalyst for selective O_2 oxidations under mild conditions actually shows more reactivity than the same quantity of the same POM catalyst in solution.[52] Therefore, our present result, the dependence of the electron configurations of POMs on their nanostructures, is also significant for the catalysis, electrochemical, and medical applications of the POM-based nanostructured materials.

Acknowledgment. This work is supported by the Key Project of National Natural Science Foundation of China (29992590-5), the Major State Basic Research Development Program (G200078102), and the Ministry of Education of China.

References and Notes

(1) Lehn, J. M. *Supramolecular Chemistry*; VCH: New York, 1995.
(2) Messer, B.; Song, J. H.; Huang, M.; Wu, Y.; Kim, F.; Yang, P. *Adv. Mater.* **2000**, *12*, 1526.
(3) Kimizuka, N.; Lee, S. H.; Kunitake, T. *Angew. Chem., Int. Ed.* **2000**, *39*, 389.
(4) Kimizuka, N. *Adv. Mater.* **2000**, *12*, 1461.
(5) Lee, C.-S.; Kimizuka N. *Proc. Natl. Acad. Sci. U.S.A.* **2002**, *99*, 4922.
(6) Camerel, F.; Antonietti, M.; Faul, C. F. J. *Chem. Eur. J.* **2003**, *9*, 2160.
(7) *Chem. Rev.* **1998**, *98*, 1. The entire issue is devoted to polyoxometalates.
(8) Pope, M. T.; Müller, A. *Polyoxometalate Chemistry from Topology via Self-Assembly to Application*; Kluwer Academic Publishers: Dordrecht, The Netherlands, 2001.
(9) Kurth, D. G.; Lehmann, P.; Volkmer, D.; Cölfen, H.; Koop, M. J.; Müller, A.; Du Chesne, A. *Chem. Eur. J.* **2000**, *6*, 385.
(10) Volkmer, D.; Du Chesne, A.; Kurth, D. G.; Schnablegger, H.; Lehmann, P.; Koop, M. J.; Müller, A. *J. Am. Chem. Soc.* **2000**, *122*, 1995.
(11) Kurth, D. G.; Lehmann, P.; Volkmer, D.; Müller, A.; Schwahn, D. *J. Chem. Soc., Dalton Trans.* **2000**, 3989.
(12) Bu, W.; Wu, L.; Hou, X.; Fan, H.; Hu, C.; Zhang, X. *J. Colloid Interface Sci.* **2002**, *251*, 120.
(13) Bu, W.; Fan, H.; Wu, L.; Hou, X.; Hu, C.; Zhang, G.; Zhang, X. *Langmuir* **2002**, *18*, 6398.
(14) Bu, W.; Zhang, J.; Wu, L.; Tang, A.-C. *Chin. J. Chem.* **2002**, *20*, 1514.
(15) Bu, W.; Wu, L.; Zhang, X.; Tang, A.-C. *J. Phys. Chem. B* **2003**, *107*, 13425.
(16) Bu, W.; Wu, L.; Tang, A.-C. *J. Colloid Interface Sci.* **2004**, *269*, 472.
(17) Bu, W.; Li, W.; Li, H.; Wu, L.; Tang, A.-C. *J. Colloid Interface Sci.* **2004**, *274*, 200.
(18) Polarz, S.; Smarsly, B.; Antonietti, M. *Chem. Phys. Chem.* **2001**, *1*, 457.
(19) Zhang, T. R.; Feng, W.; Fu, Y.; Lu, R.; Bao, C. Y.; Zhang, X. T.; Zhao, B.; Sun, C.; Li, T. J.; Zhao, Y. Y.; Yao, J. N. *J. Mater. Chem.* **2002**, *12*, 1453.
(20) Zhang, T. R.; Lu, R.; Zhang, H. Y.; Xue, P. C.; Feng, W.; Liu, X. L.; Zhao, B.; Zhao, Y. Y.; Li, T. J.; Yao, J. N. *J. Mater. Chem.* **2003**, *13*, 580.
(21) Volkmer, D.; Bredenkötter, B.; Tellenbröker, J.; Kögerler, P.; Kurth, D. G.; Lehmann, P.; Schnablegger, H.; Schwahn, D.; Piepenbrink, M.; Krebs, B. *J. Am. Chem. Soc.* **2002**, *124*, 10489.
(22) Wang, J.; Wang, H. S.; Fu, L. S.; Liu, F. Y.; Zhang, H. J. *Thin Solid Films* **2002**, *414*, 256.
(23) Wang, J.; Wang, H. S.; Liu, F. Y.; Fu, L. S.; Zhang, H. J. *J. Lumin.* **2003**, *101*, 63.
(24) Blasse, G.; Dirksen, G. J.; Zonnevijlle, F. *J. Inorg. Nucl. Chem.* **1981**, *43*, 2847.
(25) Ballardini, R.; Chiorboli, E.; Balzani, V. *Inorg. Chim. Acta* **1984**, *95*, 323.
(26) Yamase, T.; Sugeta, M. *Bull. Chem. Soc. Jpn.* **1993**, *66*, 444.
(27) Ballardini, R.; Mulazzani, Q. G.; Venturi, M.; Bolletta, F.; Balzani, V. *Inorg. Chem.* **1984**, *23*, 300.
(28) Tourné, C. M.; Tourné, G. F.; Brianso, M. C. *Acta Crystallogr.* **1980**, *B36*, 2012.
(29) Peacock, R. D.; Weakley, T. J. R. *J. Chem. Soc.* A **1971**, 1836.
(30) Wassermann, K.; Pope, M. T. *Inorg. Chem.* **2001**, *40*, 2763.
(31) Umemura, J.; Cameron, D. G.; Mantsch, H. H. *Biochim. Biophys. Acta* **1980**, *602*, 32.
(32) Sapper, H.; Cameron, D. G.; Mantsch, H. H. *Can. J. Chem.* **1981**, *59*, 2543.
(33) Rocchoccioli-Deltcheff, C.; Fournier, M.; Franck, R.; Thouvenot, R. *Inorg. Chem.* **1983**, *22*, 207.
(34) Okuyama, K.; Soboi, Y.; Iijima, N.; Hirabayashi, K.; Kunitake, T.; Kajiyama, T. *Bull. Chem. Soc. Jpn.* **1988**, *61*, 1485.
(35) Myrzakozha, D. A.; Hasegawa, T.; Nishijo, J.; Imae, T.; Ozaki, Y. *Langmuir* **1999**, *15*, 6890.
(36) Myrzakozha, D. A.; Hasegawa, T.; Nishijo, J.; Imae, T.; Ozaki, Y. *Langmuir* **1999**, *15*, 3601.
(37) Yamase, T.; Kobayashi, T.; Sugeta, M.; Naruke, H. *J. Phys. Chem. A* **1997**, *101*, 5046.
(38) Nogami, M.; Abe, Y. *J. Non-Cryst. Solids* **1996**, *197*, 73.
(39) Capobianco, J. A.; Proulx, P. P.; Bettinelli, M.; Negrisolo, F. *Phys. Rev. B* **1990**, *42*, 5936.
(40) Horrocks, W. D., Jr.; Sudnick, D. R. *Acc. Chem. Res.* **1981**, *14*, 384.
(41) Sanchez, C.; Livage, J.; Launay, J. P.; Fournier, M. *J. Am. Chem. Soc.* **1983**, *105*, 6817.
(42) Weinstock, I. A. *Chem. Rev.* **1998**, *98*, 113.
(43) Kirby, J. F.; Baker, L. C. W. *Inorg. Chem.* **1998**, *37*, 5537.
(44) Casañ-Pastor, N.; Gomez-Romero, P.; Jameson, G. B.; Baker, L. C. W. *J. Am. Chem. Soc.* **1991**, *113*, 5658.
(45) Grigoriev, V. A.; Hill, C. H.; Weinstock, I. A. *J. Am. Chem. Soc.* **2000**, *122*, 3544.
(46) Grigoriev, V. A.; Cheng, D.; Hill, C. H.; Weinstock, I. A. *J. Am. Chem. Soc.* **2001**, *123*, 5292.
(47) Matsumoto, M.; Neuman, N. I.; Swaddle, T. W. *Inorg. Chem.* **2004**, *37*, 5537.
(48) Salvatl, L., Jr.; Makovsky, L. E.; Stencel, J. M.; Brown, F. R.; Hercules, D. M. *J. Phys. Chem.* **1981**, *85*, 3700.
(49) Ng, K, T.; Hercules, D. M. *J. Phys. Chem.* **1976**, *80*, 2094.
(50) O_a: each shared by XO_4 and three octahedral from the same W_3O_{13} (X = P, Si, and B). O_b: W−O_b−W bridges between different W_3O_{13} groups. O_c: W−O_c−W bridges within the same W_3O_{13} group. O_d: terminal oxygen atom. Buckley, R. I.; Clark, R. J. H. *Coord. Chem. Rev.* **1985**, *65*, 167.
(51) Plault, L.; Hauseler, A.; Nlate, S.; Astruc, D.; Ruiz, J.; Gatard, S.; Neumann, R. *Angew. Chem., Int. Ed. Engl.* **2004**, *43*, 2924.
(52) Okun, N. M.; Anderson, T. M.; Hill, C. L. *J. Am. Chem. Soc.* **2003**, *125*, 3194.